A Kinetic Monte Carlo Study on the Nucleation Mechanisms of Oil-Soluble Initiators in the Miniemulsion Polymerization of Styrene

JONATHAN A. RAWLSTON,[1] JUCHEN GUO,[2] F. JOSEPH SCHORK,[2] MARTHA A. GROVER[1]

[1]Georgia Institute of Technology, School of Chemical and Biomolecular Engineering, 311 Ferst Dr. NW, Atlanta, Georgia 30332

[2]University of Maryland, Department of Chemical and Biomolecular Engineering, 2113 Chemical and Nuclear Engineering, College Park, Maryland 20742

ABSTRACT: The use of oil-soluble initiators in free-radical miniemulsion polymerization has increased due to their ability to generate radicals primarily within monomer droplets. Existing theories concerning the nucleation mechanism for oil-soluble initiators suggest that a single radical must be formed within a particle for propagation to occur, despite the fact that an oil-soluble initiator molecule decomposes to form two radicals. According to existing theories, the primary source of nucleating radicals may be either within the particle or from the small amount of initiator in the aqueous phase. At the nanometer size of miniemulsion particles, concentration variables do not adequately describe the reactions in a particle, and use of such variables may lead to the inaccurate description of mechanisms within a particle. Application of the kinetic Monte Carlo algorithm allows for the simulation of individual reactive events, such as propagation or termination, while tracking macroscopic observables, such as conversion and molecular weight. Comparison of the simulation results to experimental data for styrene miniemulsion polymerization indicates that desorption of radicals may be more significant at smaller particle sizes and lower reaction temperatures. Oil-soluble initiator radicals generated in the aqueous phase are found to be insignificant under typical conditions in the miniemulsion polymerization of styrene. © 2008 Wiley Periodicals, Inc. J Polym Sci Part A: Polym Chem 46: 6114–6128, 2008

Keywords: kinetics (polym.); miniemulsion polymerization; Monte Carlo simulation; particle nucleation; radical polymerization

INTRODUCTION

In conventional emulsion polymerizations, referred to here as macroemulsions, a surfactant is used to stabilize monomer droplets dispersed in water. An unseeded, batch macroemulsion poly-

merization reaction may be divided into three intervals. Particle nucleation occurs during Interval I, as radicals generated in the aqueous phase propagate and then either enter monomer-swollen micelles or precipitate from the aqueous phase and nucleate new particles. Interval I is usually completed within 2–10% monomer conversion, with most of the monomer remaining in the droplets.[1] During Interval II, polymerization occurs in the monomer-swollen particles, while the monomer concentration within the particles remains

constant due to diffusion of monomer from droplets. When the monomer droplets have disappeared, Interval III commences, and during this interval the reaction continues until the monomer in the particles is depleted.

Unpredictable particle nucleation in macroemulsions, along with the swelling of particles during Interval II, complicates control of the final particle size. Miniemulsion polymerizations overcome these issues by employing a costabilizer in addition to the surfactant, preserving the particle size from the initial dispersion by preventing decay of the monomer droplets. The droplets produced in miniemulsions are very small, on the order of 50–200 nm, and so the surface area of the droplets is quite high. Most of the surfactant is adsorbed to the droplet surfaces, rather than being free to form micelles or stabilize additional particles nucleated from the aqueous phase. Radical entry into monomer droplets, rather than micelles, is then the primary mechanism of particle nucleation, when water-soluble initiators are used.[1] Water soluble initiators dissociate into radical pairs in the aqueous phase and single radicals then enter the particles.

Although water-soluble initiators are more commonly used in miniemulsion polymerizations, due to a higher rate of polymerization, the use of oil-soluble initiators has increased in recent years.[1,2] When attempting to achieve a uniform particle size distribution, as is the case in miniemulsions, water soluble initiators present the issue of secondary nucleation, whereby additional particles may be formed from radicals in the aqueous phase. Oil-soluble initiators circumvent this obstacle by generating radicals primarily within monomer droplets, significantly decreasing the probability for secondary nucleation. A second advantage of oil-soluble initiators is greater mobility of chain ends within the particle, as the hydrophilic end-groups from water-soluble initiators are thought to remain anchored to the particle surface.[3,4] Greater mobility of the radicals allows for more complete polymerization of the particle interior, enabling the production of a uniform particle morphology. The slower rates of polymerization observed for oil-soluble initiators have been attributed to a significant fraction of radical pairs recombining within the particle immediately after dissociation. This "cage" effect may be due to the higher viscosity of the particle when compared with the aqueous phase. The fraction of initiator radicals that escape this "cage" after generation is commonly referred to as the initiator efficiency.

Even when two radicals are able to separate sufficiently within a miniemulsion particle, they are still confined to the small volume of the particle, increasing the probability of termination between these two radicals, when compared with bulk polymerizations. This confinement is thought by some authors to accelerate termination of the radicals, thereby making the existence of multiple radicals inside a particle unlikely. Therefore, the assumption is often made that either one or zero radicals are present inside a particle during the polymerization.[1] Chain-stopping occurs by either chain transfer to monomer or termination. Under the zero-one assumption, termination of radicals inside the particle is possible only when new radicals are introduced to the particle, by such means as dissociation of oil-soluble initiator or absorption of radicals from the aqueous phase. By employing a kinetic Monte Carlo (KMC) approach to model chain growth using individual monomers and radicals within a miniemulsion particle, all of these chain-stopping events may be simulated simultaneously. Our KMC simulation uses molecular rates derived directly from macroscopic rates for events that are first-order in the radical concentration, such as propagation, and chain transfer. Molecular rates that are second-order in the radical concentration, such as the termination rate, are estimated by comparison to experimental data for the monomer conversion and molecular weight. Termination of multiple radicals inside a particle is not assumed to be instantaneous, and so the zero-one assumption is not required for the KMC simulations.

As oil-soluble initiators have gained a greater foothold in miniemulsion polymerization, a debate has grown as to the primary locus of radical generation for particle nucleation. The zero-one assumption implies that the aqueous phase must be of some significance, because radicals are formed in pairs and thus should not be able to grow to a meaningful chain length without some mechanism for achieving a single radical within the particle. A small fraction of oil-soluble initiator is partitioned in the aqueous phase. Two primary schools of thought exist regarding this mechanism: one, made popular by Asua et al.,[5] poses that the locus of radical generation is within the particle, and that desorption of at least one radical must occur after initiator dissociation; the other, postulated by Nomura and Suzuki,[6] suggests that termination of radical pairs inside a particle is so overwhelming that the locus of

radical generation must be the aqueous phase, and that such radicals are subsequently absorbed into the particle.

For the desorption-dominated mechanism to be considered, radicals must first diffuse apart after generation before recombining or terminating. Radicals are unlikely to desorb from a particle after propagating several times, due to a decrease in the water-solubility of the radical, which is low from the beginning for an oil-soluble initiator radical. Asua suggests that chain transfer to monomer must occur to produce a significant number of monomeric radicals that would desorb from a particle. Desorption from a particle with a diameter of 100–200 nm is then plausible, as the growing radicals are likely to encounter the particle surface numerous times due to their high diffusivity. In one of the early studies presenting his theory, Asua et al. used a population balance model[5] to calculate the fraction of particles containing n radicals, where the maximum value of n is varied, so the zero-one assumption is not implied. Rates are calculated for radical desorption and absorption, where multiple redesorption and reabsorption steps may occur for a radical; both termination and radical generation occur in both phases. The desorption rate is calculated from the probabilities of absorption and redesorption, determined by the rates of propagation and termination in both phases. The absorption rate is determined by the diffusivity of the radicals in the aqueous phase, and a "radical capture efficiency." To solve the population balance, the number of particles containing n radicals is assumed to be at steady state. As a test system for the model, Asua et al. performed simulations for styrene at particle diameters of both 122 and 644 nm.[5] For the 122-nm particle, >99% of the particles have zero or one radical, and $\bar{n}$ is calculated to be ~ 0.5. For the 644-nm particle, >90% of the particles has three or fewer radicals, and $\bar{n}$ is found to be near 1.5. This shift in the distribution of radicals seems to indicate that radicals survive longer in a larger particle, due to decreased confinement effects. The population balance model predicts that $\bar{n}$ should be nearly 100 times higher than the $\bar{n}$ calculated from a "bulk-like" equation:

$$\bar{n} = N_A \left(\frac{k_d f n_I V_p}{k_t N_T} \right)^{0.5}, \qquad (1)$$

for particle diameters less than 100 nm. This indicates that termination may be suppressed significantly in miniemulsion particles due to compart-

mentalization of radicals into individual particles. Asua et al. varied the concentration of initiator in the aqueous phase, with the model results showing that this variation has no effect on $\bar{n}$, and therefore concludes that the locus of radical generation must be inside the particle.[5]

The absorption-dominated mechanism, posed by Nomura, requires the assumption of instantaneous termination for radical pairs produced within the particle. Oil-soluble initiators, such as 2,2'-azobis(isobutyronitrile) (AIBN), are sufficiently soluble in water to produce a substantial number of radicals in the aqueous phase at reasonable reaction temperatures. These radicals then diffuse toward particles, where they are absorbed due to their greater solubility in the particles. Nomura investigated this absorption-dominated mechanism via microemulsion polymerization of styrene using both AIBN and the water-soluble initiator potassium persulfate (KPS).[6] Microemulsion polymerization results when either the surfactant concentration is greatly increased or the monomer concentration is greatly decreased, when compared with a macroemulsion polymerization system, producing droplets of diameter 10–100 nm. Because of the difference in particle size between microemulsions and miniemulsions, a direct comparison of the particle nucleation mechanisms in microemulsions and miniemulsions is not possible. The microemulsion studies show that the rate of conversion increases with AIBN concentration, but that the rate of conversion using oil-soluble initiator is much lower than that achieved using KPS. For the microemulsions, the average molecular weight is not affected by changing the initiator concentration.[6] The findings for the conversion rate show that radical generation is the rate-limiting step in the polymerization for oil-soluble initiators, and that oil-soluble initiators exhibit lower efficiencies than water-soluble initiators. The high molecular weights observed, $6-8 \times 10^6$ g/mol, are consistent with reduced termination due to compartmentalization of radicals, and the independence of molecular weight from the rate of radical generation shows that termination occurs on a faster time scale than radical generation. For the macroemulsion study, increasing the initiator concentration is found to increase particle nucleation at similar rates for both AIBN and KPS.[6] This shows that AIBN radicals are present in the aqueous phase and are capable of nucleating new particles from the existing micelles. For the absorption-dominated mechanism to be reasonable, almost all of

the radicals generated in the aqueous phase must enter monomer-swollen micelles rather than nucleated particles, due to the relatively small number of AIBN radicals generated in the aqueous phase, when compared with the micelles. Nomura concluded that the locus of radical generation for particle nucleation in microemulsions is the aqueous phase.

EXPERIMENTAL

Past approaches to the modeling of miniemulsion particles required some level of continuum assumptions. Karlsson et al.[7] use an approach where the particles are divided into concentric shells, and the distribution of radicals is then modeled using a probability density function, based on the time of entry and fractional penetration into the particle. Other concentration variables, however, require the continuum assumption within each shell. Similarly, Asua et al.'s model[5] uses continuum assumptions for the concentration variables, but includes an integer number of radicals. Because of the submicron size of miniemulsion particles, concentration variables are not adequate to describe the amounts of different species within a particle. Using a KMC approach to model a miniemulsion particle allows for the removal of continuum variables from the simulation. Prescott used KMC to simulate chain-length dependent termination in free-radical polymerization using reversible addition-fragmentation chain transfer (RAFT).[8] Luo and Yu applied KMC to study droplet nucleation in miniemulsion polymerization using RAFT.[9] Our KMC approach simulates individual events, such as propagation, initiator dissociation, and termination, using a resolution down to the individual radical and monomer. The molecular rates for these events are either scaled directly from macroscopic rates, as for propagation and chain transfer, or else are estimated directly from experimental data, as we do for termination. This approach allows for a detailed examination of molecular-level mechanisms within the particle while tracking macroscopic observables, such as conversion and molecular weight distribution, which can be measured experimentally. Using a population balance model such as Asua et al.'s[5] with our kinetics would allow the simulation of particle conversion, but would not describe the molecular weight distribution. The solution algorithm Asua et al. used to solve the population balance model does not allow

prediction of the molecular weight distribution.[5] Simulation of the molecular weight distribution is essential to gain insight into the molecular-level mechanisms that affect particle nucleation. Having simulation data for both conversion rate and molecular weight allows us to better discriminate between the chain-stopping mechanisms. Our approach is unique in that it is the first study of the nucleation mechanisms of oil-soluble initiators in miniemulsion polymerization using KMC, and thus allows us to elucidate the dominant chain-stopping mechanisms which determine the conversion rate and molecular weight distribution.

Well-Mixed Assumption

The simulation considered here assumes that the particle is well-mixed, or of uniform consistency. This assumption is based on the center-of-mass diffusion of polymer chains being high, relative to the typical particle diameter of 100–200 nm, so that a chain could traverse the particle diameter between reactive events such as propagation. Invoking the scaling law for styrene oligomers derived by Piton et al.[10] and using a monomer diffusivity of 2.81×10^{-5} cm^2/s at 50 °C, a chain of 1000 mers would have a diffusivity of 9.53×10^{-7} cm^2/s. The styrene monomer diffusivity at 50 °C is determined by taking the diffusivity at 25 °C[11] and scaling it with an Arrhenius law, where the activation energy used is for the diffusivity of toluene in polystyrene.[12] Using a propagation rate constant of 1999 s^{-1}, a chain of 1000 mers could achieve center-of-mass movement of 535 nm between propagation events at 0% monomer conversion. A chain length of 1000 requires extrapolation of the diffusivity relation, but for shorter chains, the diffusion distance is even longer. The gel effect for styrene is shown by both our data and Alduncin and Asua's data[13] to be negligible, as the acceleration in the conversion rate characteristic of the gel effect is not observed in these conversion-time data. This lack of a gel effect in styrene shows that a significant decrease in radical diffusivity does not occur until >90% monomer conversion, when the glass effect is observed, as reactive diffusion of the radicals is slowed. Thus, the assumption of a well-mixed particle is justified in this study. The simulations discussed here are for a single particle, which is possible because miniemulsion particles are generally decoupled from each other, due to the presence of the costabilizer.

Table 1. Macroscopic and Molecular Rate Equations

Rate	Macroscopic	Units	Molecular	Units
r_p	$k_p[R^*][M]$	mol/L/s	$k_{p,m}N_{m,0}n$	s^{-1}
r_{tr}	$k_{tr}[R^*][M]$	mol/L/s	$k_{tr,m}N_{m,0}n$	s^{-1}
r_d	$k_d[I]$	s^{-1}	$k_{d,m}N_I$	s^{-1}
r_t	$k_t[R^*]^2$	mol/L/s	$k_{t,m}N_{pairs}$	s^{-1}
r_{abs}	–	–	$k_{abs,m}n_{aq}$	s^{-1}
r_{des}	–	–	$k_{des,m}n$	s^{-1}

Propagation, Chain Transfer, Initiator Dissociation

In the current simulations for styrene, the rate constants for propagation,[14] chain transfer,[15] and initiator dissociation[16] are calculated, respectively, according to:

$$k_p = 4.27 \times 10^7 \exp\left(\frac{-32.51}{RT}\right), \qquad (2)$$

$$k_{tr} = 2.0 \times 10^7 \exp\left(\frac{-56.7}{RT}\right), \qquad (3)$$

$$k_d = 1.29 \times 10^{15} \exp\left(\frac{-127.6}{RT}\right), \qquad (4)$$

where k_p and k_{tr} are in L/mol/s, k_d is in s^{-1}, and the activation energies are in kJ/mol. The macroscopic and molecular rate equations for these events are shown in Table 1, where n and N_I are the number of radicals and initiator molecules in the particle, respectively.

The rate constants for the second-order reactions are scaled down to the molecular level by multiplying by the concentration of styrene in the particle, $[M] = N_m/(V_pN_A)$, where N_m is the number of monomers in the particle, V_p is the particle volume, and N_A is Avogadro's number. The molecular rate constant for propagation is calculated as $k_{p,m} = k_p/(V_pN_A)$, and the molecular rate constant for chain transfer is likewise calculated as $k_{tr,m} =$ $k_{tr}/(V_pN_A)$. As the number of monomers in the particle decreases, the rates of propagation and chain transfer decrease. The initial concentration of styrene, $[M]_0$, in the particle is determined from the density and molecular weight. The molecular weight of styrene is 104.15 g/mol, and the density at 75 °C is 855.2 g/L,[17] giving an initial monomer concentration of 8.21 mol/L. The molecular initiator dissociation rate constant $k_{d,m}$ is equal to the macroscopic rate constant k_d. The macroscopic and molecular rate constants at 75 °C are shown in Table 2.

Termination

The macroscopic termination reaction is second-order in the concentration of radicals within a particle, as shown in Table 1. The macroscopic termination rate constant is calculated according to:

$$k_t = 1.3 \times 10^9 \exp\left(\frac{-9.92}{RT}\right), \qquad (5)$$

where k_t is in L/mol/s and the activation energy is in kJ/mol.[18] The macroscopic termination rate constant at 75 °C is given in Table 2. For the purposes of the KMC simulations, at least two radicals must be present inside a particle for termination to occur. The molecular termination rate is calculated as shown in Table 1, where N_{pairs} is the number of possible radical pairs, and possible termination events, within the particle, and the molecular termination rate constant is

$$k_{t,m} = k_t[R^*], \qquad (6)$$

where the value for $[R^*]$ is the concentration of two radicals in a particle, $2/(V_pN_A)$. Two radicals are equal to 3.32×10^{-24} moles, and assuming a particle diameter of 100 nm gives a particle volume of 5.24×10^{-9} L, so the concentration

Table 2. Macroscopic and Molecular Rate Constants for Styrene at 75 °C and 0% Conversion

Mechanism	Macroscopic	Units	Molecular	Units
Propagation	5.65×10^2	L/mol/s	3.65×10^{-4}	s^{-1}
Chain transfer	6.22×10^{-2}	L/mol/s	4.01×10^{-8}	s^{-1}
Initiator dissociation	9.24×10^{-5}	s^{-1}	9.24×10^{-5}	s^{-1}
Termination	4.21×10^7	L/mol/s	–	s^{-1}
Absorption	–	–	3.07	s^{-1}
Desorption	–	–	–	s^{-1}

corresponding to two radicals in a 100-nm particle is 6.34×10^{-6} mol/L. The molecular termination rate constant $k_{t,m}$ is then 267 s^{-1}. If the particle diameter is increased to 170 nm, the concentration for two radicals drops to 1.29×10^{-6} mol/L, giving a molecular termination rate constant of 54.3 s^{-1}. Because of its variation with particle size, no value for $k_{t,m}$ is given in Table 2. For styrene, termination occurs by combination of the radicals (not disproportionation), and this will be implied throughout the remainder of the discussion.

Radical Absorption and Desorption

For radical absorption to occur, we assume that a critical chain length for radical entry must be reached, such that the radical no longer has sufficient water-solubility to remain in the aqueous phase. Thus, the time for a radical to reach the critical length for entry is dependent on the rate of propagation in the aqueous phase. Direct calculation of a macroscopic absorption rate constant is not straightforward, and so no macroscopic value is given in Table 2, but the molecular value is estimated here. The concentration of styrene in the aqueous phase is calculated to be 0.0566 g sty/100 mL H$_2$O, based on a fit to literature data.[19] The concentration of styrene in the aqueous phase is then calculated as $0.0566 \times (10/MW_{sty}) = 5.44 \times 10^{-3}$ mol/L. For styrene, the critical length for radical entry is 2 mers,[20] and when using AIBN, the initiator radical is close in size to a monomer, and so an aqueous-phase radical need only propagate once to reach the critical length for entry. The absorption rate constant, shown in Table 2, is then calculated as $k_{p,m}$ times the aqueous-phase styrene concentration. The molecular absorption rate is calculated as shown in Table 1. However, because AIBN is oil-soluble, it may adsorb even sooner, and so this absorption rate is considered to be a lower bound on the actual value. We investigate and evaluate this effect and assumption both in the simulation study and in comparison with the experiments. To examine the two competing mechanisms for particle nucleation, the simulation of desorption and absorption events must be carefully considered to require as few assumptions as possible, while ensuring that any remaining assumptions are justified. As previously stated, at the particle diameters considered here, both monomeric and initiator radicals diffuse at high enough rates to encounter the particle surface multiple times before propagating. Desorption may therefore be allowed for both such

types of radicals, but it is not allowed for radicals of length greater than one, because these radicals will be either at or beyond the critical chain length for radical entry.[20] Rate constants for radical desorption in the literature generally incorporate the chain transfer rate, because many authors assume that monomeric radicals, rather than initiator radicals, are the primary desorbing species.[5,6] The molecular desorption rate, as shown in Table 1, is only dependent on n, the number of radicals in the particle. Within the KMC simulation, k_{des} is estimated using multiples of $k_{p,m}N_{m,0}$, to vary the fraction of radicals that desorb, and so no value for k_{des} is given in Table 2. For radicals that are generated in the aqueous phase, absorption is the only event allowed in the simulation, where the rate of absorption, as previously explained, is determined by the time to reach the critical chain length for radical entry. The simulation results presented here do not include absorption of radicals from the aqueous phase.

From the recipe information for the two experimental data sets used for comparison, the concentrations of AIBN in the particle are 0.127 mol/L for Alduncin and Asua's data set[13] and 6.10×10^{-2} mol/L for our data set. Using a partition coefficient of 115, the value for AIBN at 50 °C,[21] the aqueous phase concentrations of AIBN are, respectively, 1.10×10^{-3} and 5.30×10^{-3} mol/L. Using a 100-nm particle for Alduncin and Asua's data set,[13] the number of AIBN molecules per particle is calculated to be 40,068. Based on Alduncin and Asua's recipe information,[13] the volume of water per particle is calculated to be 1.45×10^{-18} L, and so the number of AIBN molecules in the aqueous phase per particle is 962. The initial rates of dissociation for this system are therefore 3.7 s^{-1} in the particle and 8.9×10^{-2} s^{-1} in the aqueous phase. Taking the same approach with a 109-nm particle and our recipe, the initial rates of AIBN dissociation are 7.6×10^{-2} s^{-1} in the particle and 3.2×10^{-3} s^{-1} in the aqueous phase. Comparison of the aqueous-phase dissociation rate to the absorption rate in both cases shows that absorption is much faster than initiator dissociation, such that generation of aqueous-phase radicals would be the rate-limiting step. For Alduncin and Asua's recipe[13] using a 170-nm particle, two radicals in the volume of 7.10×10^{-18} L per particle give a radical concentration of 4.67×10^{-7} mol/L. This gives a microscopic termination rate of 19.7 s^{-1}, so the termination rate is sufficiently small to neglect termination in the aqueous phase. Because of the low concentration of
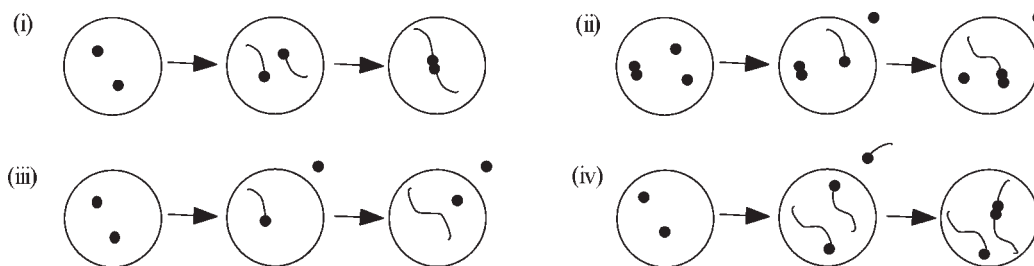
Figure 1. Possible chain-stopping mechanisms: simple termination (i), termination by initiator dissociation (ii), chain transfer to monomer (iii), and termination by absorption (iv).

radicals in the aqueous phase, termination in the aqueous phase is typically neglected. Although radicals generated in the aqueous phase are allowed to adsorb, the overall fraction of these radicals is much smaller than the number of radicals generated in the particle.

KMC Algorithm

Events within the particle are selected randomly according to the KMC algorithm,[22,23] depending upon the number of live chains within the particle. The total sum of rates for all possible events is calculated by

$$K_{\text{sum}} = \sum_{i=1}^{N} E_i K_i, \tag{7}$$

where E_i is the number of possible events of type i for the current population of live chains, and K_i is the molecular rate constant for each event of type i, the values of which are shown in Table 2. Each product $E_i K_i$ represents a bin for event i relative to the total K_{sum}. A uniformly distributed random number is selected using the Mersenne Twister random number generator, and the bin in which the random number is located determines the event to be executed. The time step for each event is determined by:

$$\tau = \frac{-\ln(x_r)}{K_{\text{sum}}}, \tag{8}$$

where x_r is a uniformly distributed random number in the interval (0,1]. After each event is executed, the arrays describing the lengths of all live and dead chains are updated, and E_i is recomputed—K_i remains constant throughout.

Chain-Stopping Mechanisms

To form an initial hypothesis regarding the nucleation mechanism, a number of possible chain-stopping mechanisms are considered, using the molecular rate constants to predict the molecular weight produced from each chain-stopping event. By comparing these predicted molecular weights to those observed in the experimental data sets, we gain insight into the more plausible chain-stopping mechanisms. These mechanisms are illustrated in Figure 1. Simple termination (i) involves the simultaneous propagation of a pair of radicals, followed by termination between the pair. For termination by initiator dissociation (ii), one dissociation event occurs, which could be followed by desorption of one of the radicals. The remaining radical propagates, until the next dissociation occurs and the growing chain is terminated by a newly generated radical. As more initiator molecules dissociate, the time between dissociations increases, not only making this mechanism less likely, but also increasing the chain lengths for radicals terminated in such a manner. Chain-stopping via chain-transfer (iii) would most likely occur after desorption of one radical of a pair, followed by growth of the remaining radical until chain transfer to monomer occurs, producing a dead chain. The length of this chain depends on the ratio of the propagation rate to the chain transfer rate, k_p/k_{tr}. For termination by absorption (iv), a radical enters the particle from the aqueous phase and terminates the radical on a live polymer chain. This mechanism is commonly referred to as short-long termination.

For Asua's styrene miniemulsion polymerization at 75 °C, the peak of the molecular weight probability density distribution is approximately 1.26×10^4 g/mol at 30% particle conversion, giving a chain length of 121 mers. Based on Alduncin and Asua's measurements of particle size,[13] comparison to this case will be made using a 170-nm particle. For mechanism (i), simple termination, the initial degree of polymerization is predicted as

$2k_{p,m}N_{m,0}/k_{t,m}$, where $k_{p,m}$ and $k_{t,m}$ are the molecular propagation and termination rates, respectively. This gives a chain length of 171 mers for mechanism (i), which is larger than the experimental chain length of 121 mers, but in the same order of magnitude, and so this mechanism cannot be eliminated. To predict the chain length for mechanism (ii), the initial time between initiator dissociations is used. There are 1.97×10^5 AIBN molecules in a 170-nm particle, and so the initial time between dissociations is 5.50×10^{-2} s. Multiplying this time by $k_{p,m}N_{m,0}$ gives an initial estimate for the expected chain length for mechanism (ii) of 255 mers. This is larger than the experimental chain length, but again in the same order of magnitude, so this mechanism also could be significant. For mechanism (iii), the chain length is the ratio $k_{p,m}N_{m,0}/k_{tr,m}$, or 9.09×10^3 mers. This chain length is much higher than the experimental data, so it seems unlikely that mechanism (iii) is significant in the polymerization. Because of this relatively low value of $k_{tr,m}$ compared with the other rates, chain transfer is usually considered to be insignificant for styrene. For mechanism (iv), the lifetime of the growing radical is determined from the absorption rate, given in Table 2, to be 3.25×10^{-1} s. This gives a chain length for mechanism (iv) of 1.51×10^3, much higher than that observed experimentally, and so mechanism (iv) is unlikely to contribute significantly, unless reabsorption is actually occurring at a substantially higher rate. The two most plausible chain-stopping mechanisms are clearly mechanisms (i) and (ii), although (iv) cannot be ruled out without considering further information on the absorption rate. By comparing the molecular rate of termination with the initial time between initiator dissociations, the observation is made that dissociation occurs faster than termination, and so desorption of a radical may not be necessary for mechanism (ii) to occur. Based on these predictions of degree of polymerization, the hypothesis is formed that aqueous-phase radicals are likely insignificant in the miniemulsion polymerization of styrene, and that multiple radicals may coexist inside a particle to propagate chains of a statistically significant length. We will investigate and quantify these arguments using the KMC simulations and experimental data.

Experimental Procedure

To test the hypothesis that aqueous-phase radicals are insignificant in the miniemulsion poly-

Table 3. Recipe Information for Miniemulsion Polymerizations

	A	B	C	D
Temperature (°C)	50	50	40	40
Styrene (g)	20	20	–	–
Butyl acrylate (g)	–	–	25	25
KPS (g)	–	–	0.375	0.375
AIBN (g)	0.228	0.228	–	–
SDS (g)	0.8	0.8	0.8	0.8
Hexadecane (g)	1	1	1	1
NaNO$_2$ (g)	–	1.66	–	1.66
Water (g)	110	110	110	110

merization of styrene, we conducted experiments to determine the effect of such radicals on both the rate of conversion and the molecular weight distribution. This confirmation is needed to more conclusively eliminate mechanism (iv), because the rates of radical desorption and adsorption are not well known. The recipes for these experiments are shown in Table 3, and the following standard procedure is used. Styrene and butyl acrylate (BA) were purchased from Sigma-Aldrich, and the inhibitors in styrene and BA were removed by the inhibitor-remover column (from Sigma-Aldrich) before use. Sodium dodecyl sulfate (SDS), KPS, AIBN, sodium nitrite (NaNO$_2$), hydroquinone and hexadecane were all purchased from Sigma-Aldrich and used as received. The costabilizer (hexadecane) and oil-soluble free radical initiator (AIBN) are dissolved in the monomer mix. The surfactant (SDS) is dissolved in deionized water. When water-soluble initiator (KPS) is used, a part of the recipe's total water (10%) is reserved for preparation of the KPS solution. By dispersing the oil phase into the surfactant aqueous solution with a magnetic stirrer, a coarse emulsion is created, which is then sonicated with an OmniRuptor 250 Ultrasonic Homogenizer for 6 min at 20% power output (30 W) to form a miniemulsion. The miniemulsion is then transferred into a standard glass resin kettle equipped with nitrogen purge, reflux condenser, thermometer and paddle stirrer. Under nitrogen purging to remove oxygen from the miniemulsion and the reactor headspace, the reaction material is heated using a water bath to the polymerization temperature, 40 °C for KPS initiation and 50 °C for AIBN initiation. For KPS, time zero is the time at which the KPS solution is injected into the reactor. For AIBN, time zero is defined as the time at which the reactor is immersed in the water bath. The polymerization

is carried out under nitrogen purging and at an impeller speed of 300 rpm. At intervals, samples of the reactor contents are removed by syringe and put in vials containing small quantities of 0.5 wt % hydroquinone solution which functions to quench the polymerization by scavenging free radicals. Monomer conversion is measured offline by gravimetric analysis of the samples. Following the polymerization experiments, the molecular weight and molecular weight distribution of the samples were measured by gel permeation chromatography (GPC) with a Waters 410 differential refractometer operated at 30 °C. HPLC grade chloroform was used as the solvent carrier (0.6 mL/min).

RESULTS AND DISCUSSION

Experimental Results

In experiments (B) and (D), $NaNO_2$ was added as an aqueous-phase radical scavenger, to destroy both radicals desorbed from particles and radicals generated in the aqueous phase. The polymerizations using BA and KPS were conducted as a control, to show the effectiveness of the $NaNO_2$ in destroying aqueous-phase radicals. In experiment (B), the ratio of $NaNO_2$ molecules to AIBN radicals is 8.7, considering that each $NaNO_2$ molecule can only scavenge one AIBN radical, and each AIBN molecule produces two radicals. Figure 2 shows that the rate of conversion for styrene using AIBN is similar both with and without $NaNO_2$, indicating that absorption of aqueous-phase radicals is insignificant in the miniemulsion polymerization of styrene. A significantly different conversion rate when using $NaNO_2$ would indicate that the aqueous-phase radicals contribute to the polymerization, but this is not observed for the two sets of data using styrene in Figure 2. If radicals are present in the aqueous phase due to desorption, then the readsorption of these radicals should be insignificant based on the data in Figure 2. This observation concerning the insignificance of aqueous phase radicals justifies the assumption to neglect aqueous-phase termination, as well as radical absorption, in the KMC simulations. If these radicals are not significant in the polymerization, then their reactions in the aqueous phase should not significantly affect the polymerization. The initial lag in the conversion curve using $NaNO_2$ is thought to be due to a small amount of $NaNO_2$ present in the particles, which must be consumed before propagation can begin.
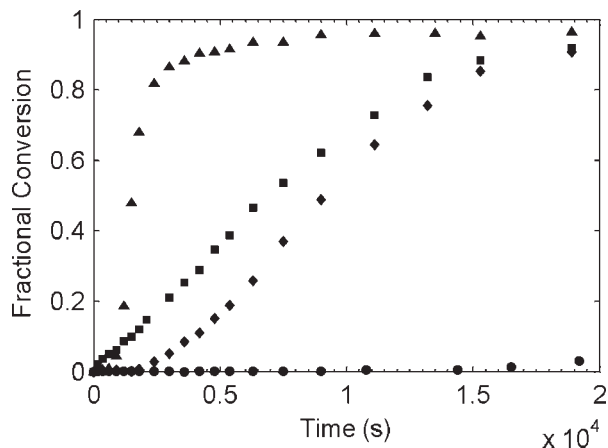
Figure 2. Experimental conversion versus time for miniemulsions of styrene and AIBN both with (◆) and without (■) $NaNO_2$ at 50 °C and for miniemulsions of butyl acrylate and KPS both with (●) and without (▲) $NaNO_2$ at 40 °C.

As Figure 2 shows, the polymerization using BA and KPS is suppressed almost entirely when using $NaNO_2$. The peak of the molecular weight probability density distribution for experiment (A) is about 5.21×10^5 g/mol, or about 5000 mers, and the particle diameter is measured to be 109 ± 0.4 nm. For experiment (B), the peak molecular weight is about 6.40×10^5 g/mol, or about 6140 mers, and the particle diameter is measured to be 104 ± 0.4 nm. The polydispersity index of the particle size for these experiments is expected to be small, around 1.1 or less.

Considering the peak molecular weight from experiment (A), each of the chain-stopping mechanisms should be examined, to determine which is most consistent with our data. Based on our experimental data and the arguments in the "Results and Discussion" section, chain-stopping mechanism (iv) should not be significant for our data, because this requires adsorption of radicals from the aqueous phase. The initial molecular propagation rate for styrene at 50 °C is 1999 s^{-1} per radical, and the molecular termination rate is 158 s^{-1}, for our particle diameter of 109 nm. The predicted molecular weight for mechanism (i), simple termination, is $2k_{p,m}N_{m,0}MW_{sty}/k_{t,m}$, or 2.63×10^3 g/mol, significantly less than the peak molecular weight for experiment (A). From the recipe for experiment (A), the number of AIBN molecules in a 109-nm particle is calculated as 2.49×10^4 molecules. The dissociation rate of AIBN at 50 °C is 3.05×10^{-6} s^{-1}, and so the initial time between initiator dissociations,

assuming an efficiency of 1, is 13.2 s. Thus, the molecular weight predicted for mechanism (ii) is 2.74×10^6 g/mol, and when the efficiency is decreased to a more realistic value of 0.5, the molecular weight doubles to 5.48×10^6 g/mol, much higher than the peak molecular weight for experiment (A). At 50 °C, the chain transfer rate is 0.115 s^{-1}, and so the molecular weight expected for mechanism (iii) is 1.81×10^6 g/mol, closer to the experimental molecular weight than the predictions for both mechanisms (i) and (ii). In other words, chain transfer should occur for most chains, prior to decomposition of a new initiator molecule, leading to a molecular weight consistent with experiments (A) and (B). The difference in molecular weight between experiments (A) and (B) is larger than the expected variability between runs, and so the residual NaNO$_2$ seems to have some effect on the molecular weight. Residual NaNO$_2$ could result in the formation of more single radicals in the particle, thus reducing the effect of mechanism (iii) on the molecular weight, allowing mechanism (ii) to be more significant. The expected dominance of mechanism (iii) implies that radical desorption must be significant, so that mechanism (i) termination will not occur. Chain transfer to monomer should be the dominant chain-stopping mechanism to achieve agreement with the peak molecular weight for experiment (A), with mechanism (ii) possibly playing a secondary role.

Simulation Results

Simulated molecular weight using the conditions of our experiments is shown in Figure 3 along with the molecular weight data from experiment (A). To calculate each molecular weight distribution, all of the chains of molecular weight greater than 1000 g/mol from 100 individual particle simulations are sorted into bins equally spaced on a log scale, as observed in Figure 3. The weight of the chains in a bin is divided by the weight of all chains included in the distribution, and this weight fraction is then divided by the fractional width of the bin in terms of the true scale, because the bins are equally spaced on a log scale. Chains at lower molecular weights are thus weighted more heavily in the distribution. In the case of the data from experiment (A), the weight fractions are determined from the GPC data, and so the weight fractions are scaled according to the relative bin size on the true scale. The area under the curve is then normalized to one to allow for a
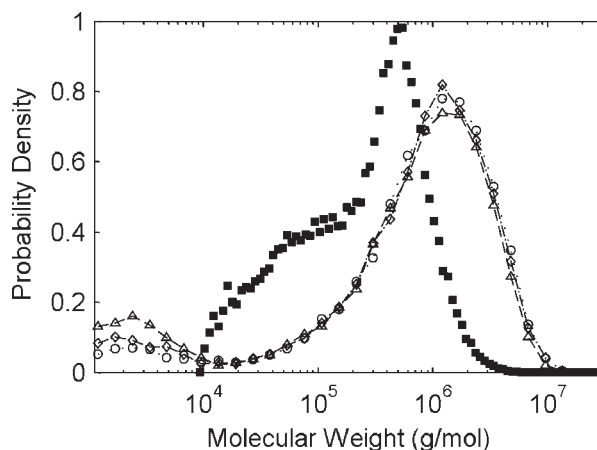
Figure 3. Normalized density of molecular weight distribution from KMC simulation, for a particle diameter of 109 nm at 50 °C and 30% particle conversion, using $k_{t,m} = 158$ s^{-1}, $f = 0.6$, and desorption rates of 2.0 $k_{p,m}N_{m,0}$ ($\triangle$) (dashed line); 3.5 $k_{p,m}N_{m,0}$ ($\diamond$) (dash-dot line); 5.0 $k_{p,m}N_{m,0}$ ($\bigcirc$) (dotted line), compared with normalized density of experiment (A) at final conversion of 92%.

better comparison to the experimental data. Given the assumptions of our model, we do not look for perfect agreement between the simulated molecular weight and the experimental molecular weight, but instead for qualitative agreement such as alignment of the peaks of the molecular weight distributions. Simple termination is 10^3 times faster than chain transfer in a 109-nm particle with two radicals, and so single radicals must be present within the particle in order for chain transfer to dominate the molecular weight. Because, by our experiments, adsorption of radicals from the aqueous phase is shown to be insignificant, a single radical must be formed via desorption of the other radical produced by an initiator dissociation in the particle. The peak molecular weights for all of the simulation data in Figure 3 are near 1×10^6 g/mol, which is close to the predicted molecular weight for mechanism (iii). Minimal variation in the molecular weight peak is observed as the desorption rate is varied, due to the long time between initiator dissociations. The difference in the experimental and simulated molecular weight distributions may be explained by the scatter in the measured chain transfer rates, almost an order of magnitude near the experimental temperature.[15] Although the initiator efficiency can also affect the molecular weight distribution, this effect should be minimal if mechanism (iii) is dominant, and so we choose to vary
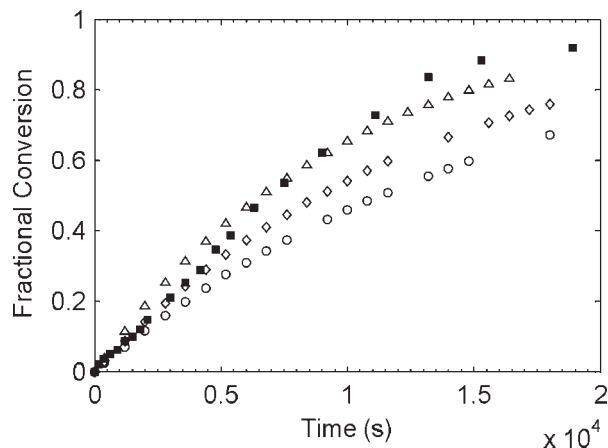
Figure 4. Conversion versus time from KMC simulation, for a particle diameter of 109 nm at 50 °C, using $k_{t,m} = 158$ s^{-1}, $f = 0.6$, and desorption rates of 2.0 $k_{p,m}N_{m,0}$ ($\triangle$); 3.5 $k_{p,m}N_{m,0}$ ($\diamond$); 5.0 $k_{p,m}N_{m,0}$ ($\bigcirc$), with our data from exp. (A) ($\blacksquare$).

the desorption rate at a constant initiator efficiency of 0.6 when comparing the KMC simulations to our experimental data. The secondary peak observed in Figure 3 decreases as the desorption rate is increased. Both the initiator efficiency and the desorption rate affect the conversion rate, and so they may not be estimated independently.

Up to a molecular weight of 2×10^5 g/mol, a shoulder is observed in Figure 3 for the data from experiment (A). Examination of the molecular weight density distribution for experiment (B) reveals that this shoulder is not present when NaNO$_2$ is used to destroy aqueous-phase radicals. For our experimental conditions, the absorption rate is estimated to be 1.00 s^{-1}, giving a predicted molecular weight of 2.08×10^5 g/mol for mechanism (iv), when one radical from a pair desorbs and is subsequently reabsorbed, resulting in short-long termination. When absorption of radicals is allowed, the peak molecular weight shifts down to 1.52×10^5 g/mol, close to the predicted molecular weight for mechanism (iv). Reabsorption of desorbed radicals is likely responsible for the shoulder observed in Figure 3, thus indicating that absorption of radicals has a minor effect on the polymerization. Fewer chains are produced via mechanism (iv) than by mechanism (iii), and the chains produced via mechanism (iv) are also shorter, and so mechanism (iv) is not significant in the rate of conversion.

When comparing the simulated conversion rate to that of the experimental data, our primary focus is on achieving agreement with the early conversion rate, up to about 30% conversion. The comparisons of the KMC simulations to both our experimental data and Asua's are made at particle conversions well below the gel point for styrene, and so neither the gel nor the glass effects should be necessary for the simulation to accurately predict the MWD at these conversions. Figure 4 shows conversion versus time results from the simulations in comparison to our data from experiment (A). Using a desorption rate around $3.5k_{p,m}$ gives good agreement with the initial conversion rate from experiment (A). Initiator efficiency and desorption rate are somewhat correlated when comparing the simulated and experimental conversion rate. Increasing the desorption rate decreases the rate of conversion, due to the corresponding decrease in the number of radicals in the particle, as radicals are not allowed to reenter the particle after desorbing. Thus, an increased desorption rate gives the same effect as a decreased initiator efficiency. Conversely, if the initiator efficiency were increased from 0.6, then a desorption rate greater than $3.5k_{p,m}$ would be required to achieve agreement with the early conversion rate.

Simulation results for a particle diameter of 170 nm at a temperature of 75 °C are shown in Figures 5–7, where each data set is an average of 100 single particle simulations. This temperature is used to correspond to Alduncin and Asua's
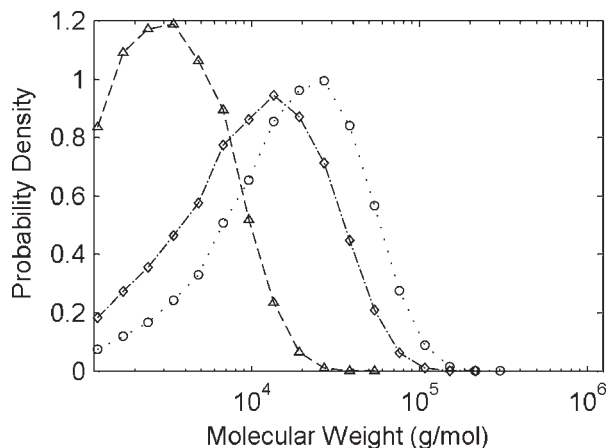
Figure 5. Normalized density of molecular weight distributions from KMC simulation using styrene at 75 °C, at 19% particle conversion and various particle sizes, with zero desorption, $k_p = 5.65 \times 10^2$ L/mol/s, $k_t = 4.21 \times 10^7$ L/mol/s, $k_d = 9.24 \times 10^{-5}$ s^{-1}, $f = 0.6$. Particle diameters of 100 nm ($\triangle$) (dashed line); 170 nm ($\diamond$) (dash-dot line); 240 nm ($\bigcirc$) (dotted line).
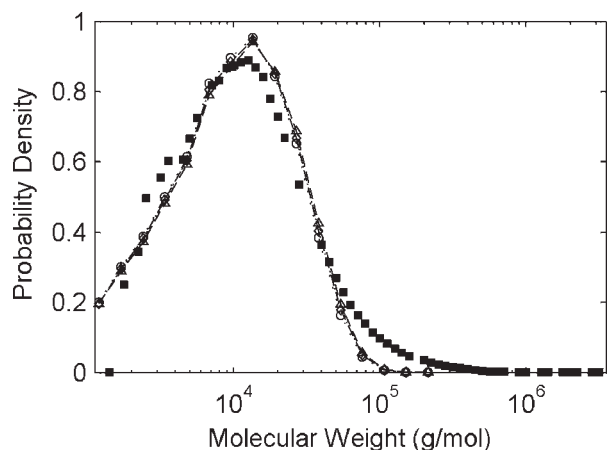
Figure 6. Normalized density of molecular weight distributions from KMC simulation using styrene at 75 °C, at 30% particle conversion and a particle diameter of 170 nm, with $k_{t,m} = 54.3$ s^{-1} and initiator efficiencies of 0.45 ($\triangle$) (dashed line); 0.6 ($\diamond$) (dash-dot line); 0.75 ($\bigcirc$) (dotted line), with Alduncin and Asua's MWD data[13] at 30% conversion ($\blacksquare$).

experimental conditions.[13] The particle size distribution for Alduncin and Asua's data[13] encompasses a significant range of particle sizes. Although most of the particles at 30% conversion, where the simulated molecular weight distributions are compared, have diameters of 100–200 nm, a small fraction of the particles may have a diameter greater than 1000 nm.[13] At higher conversion the distribution is even broader, and so we compare the molecular weight distributions at 19% conversion for Figure 5. The initiator efficiency of 0.6 used in Figure 5 is chosen due to the agreement it produces with Alduncin and Asua's experimental data[13] for both the peak molecular weight in Figure 6 and the early conversion rate in Figure 7. The data shown in Figure 5 illustrate the importance of particle size on the molecular weight distribution, because a single pair of radicals will take longer to terminate in a larger particle. Increasing the particle diameter from 100 to 170 nm produces nearly an order-of-magnitude increase in the molecular weight peak. The predicted molecular weight for chain-stopping mechanism (i), simple termination, is $2k_{p,m}N_{m,0}MW_{sty}/k_{t,m}$, which is 3.6×10^3 g/mol for a 100-nm particle, and 1.8×10^4 g/mol for a 170-nm particle. Both of these MWs are consistent with the simulated molecular weight peaks in Figure 5. For the 240-nm particle, mechanism (i) predicts a molecular weight of 5.0×10^4 g/mol, whereas mechanism (ii) predicts a molecular

weight of 2.4×10^4 g/mol. Figure 5 shows that the molecular weight peak for the 240-nm particle is between the molecular weights predicted by mechanisms (i) and (ii), and so the molecular weight distribution shown in Figure 5 appears to be an average of these two mechanisms. For the 170-nm particle, mechanism (ii) predicts a molecular weight of 6.7×10^4 g/mol, and so the molecular weight predicted by mechanism (i) for the 170-nm particle is likely more significant for the peak molecular weight shown in Figure 5 for this particle size, although mechanism (ii) may also contribute to the molecular weight. For the 100-nm particle, mechanism (ii) predicts a molecular weight of 3.3×10^5 g/mol, much higher than that predicted for this particle size by mechanism (i). Although the molecular weight predicted by mechanism (ii) is higher than the secondary peak for the 100-nm particle in Figure 5, mechanism (ii) may be partly responsible for producing this peak, due to the stochastic nature of the simulations. The molecular weight predicted by mechanism (iii), chain transfer, is 9.46×10^5 g/mol, considerably higher than all of the peaks observed in Figure 5, and so mechanism (iii) should not contribute significantly to any of these molecular weight peaks. Simple termination is dominant for the 100-nm particle and also a primary contributor for the 170-nm particle. Increasing the particle size shortens the time between initiator dissociations, and so mechanisms (i) and (ii) are equally significant for the diameter of 240 nm. Initiator efficiency has a small effect on the molecular
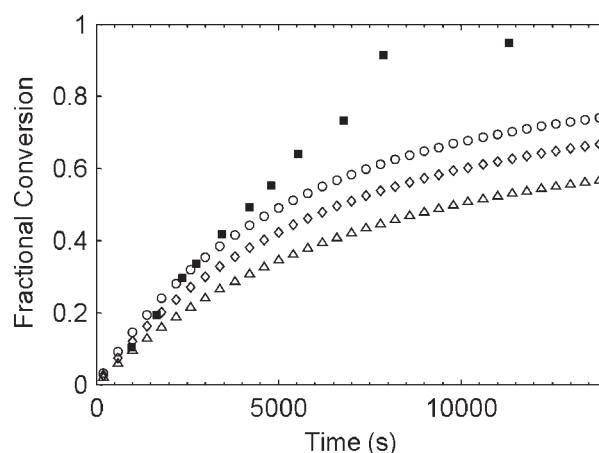
Figure 7. Conversion versus time from KMC simulation using styrene at 75 °C and a particle diameter of 170 nm, with $k_{t,m} = 54.3$ s^{-1} and initiator efficiencies of 0.45 ($\triangle$); 0.6 ($\diamond$); 0.75 ($\bigcirc$), with Alduncin and Asua's conversion versus time data[13] ($\blacksquare$).
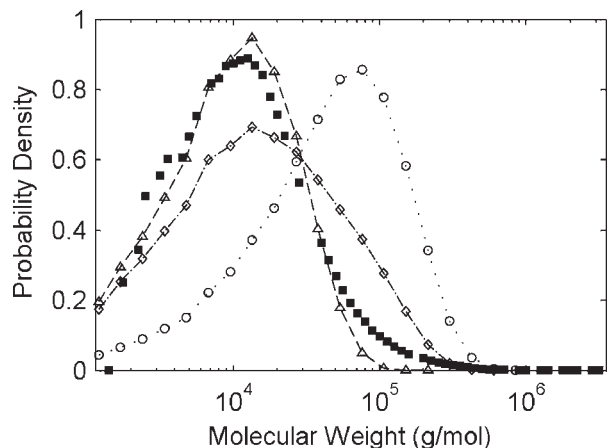
Figure 8. Normalized density of molecular weight distributions from KMC simulation using styrene at 75 °C, at 30% particle conversion and a particle diameter of 170 nm, with $k_{t,m} = 54.3$ s^{-1}, $f = 0.6$, and desorption rates of 0.0 ($\triangle$) (dashed line); 0.05 $k_{p,m}N_{m,0}$ ($\diamondsuit$) (dash-dot line); 3.0 $k_{p,m}N_{m,0}$ ($\bigcirc$) (dotted line), with Alduncin and Asua's MWD data[13] at 30% conversion ($\blacksquare$).

weight as long as mechanism (i) is dominant. A particle diameter of 170 nm is chosen for Figures 6 and 7 because this gives a value for $k_{t,m}$ of 54.3 s^{-1}, allowing the peak of the simulated MWD to agree with the peak of Asua's MWD,[13] as shown in Figure 6.

In Figure 7, the rate of conversion is shown to increase with initiator efficiency. As effective radicals are produced at a faster rate, the observed rate of polymerization increases. Figure 6 shows that the molecular weight distribution remains nearly unchanged as the initiator efficiency is increased, indicating the dominance of mechanism (i). As effective radicals are produced at a faster rate, mechanism (ii) becomes more dominant compared with mechanism (i), but this effect is reduced at smaller particle sizes due to the smaller amount of initiator initially present. In both Figures 6 and 7, using an initiator efficiency of 0.6 and no desorption provides good agreement with Asua's experimental data, for both early conversion rate and molecular weight. Because of the significant coarsening of the particle size after 30% conversion, we do not attempt to match the data beyond 30%. Initiator efficiency has a significant effect on the rate of conversion, but its effect on the molecular weight is much smaller, provided that mechanism (i) is dominant. Because Figure 6 shows that molecular weight is only slightly affected by changes in initiator efficiency, we conclude that mechanism (i) is dominant for

our chosen particle diameter of 170 nm. Next, we examine the effects of radical desorption in the KMC simulation in comparison to Asua's experimental data.

Figures 8 and 9 show that a negligible amount of desorption is allowable to attain the same early rate of conversion as observed in Asua's experimental data. When desorption is allowed to occur, single radicals formed in the particle grow unchecked until the next initiator decomposition. This produces an increase in the peak molecular weight, as well as an increase in the conversion rate. In comparing the simulations at Asua's experimental conditions to those at our experimental conditions, the two experiments appear to be in different regimes. Simple termination appears to dominate the molecular weight in Asua's experiments, whereas chain transfer is shown to dominate the molecular weight in our experiments. This difference is due to an apparent lack of radical desorption suggested by Asua's experimental data. If desorption does occur in Asua's experimental data, it must be followed quickly by readsorption, with no tangible effect on the polymerization. The probability of a radical escaping the particle before propagating, as required by our KMC simulation, is affected by both the temperature and the particle size. Because the propagation rate scales faster with temperature than does the diffusivity, the probability of escaping a particle of equal volume should decrease as the temperature increases.
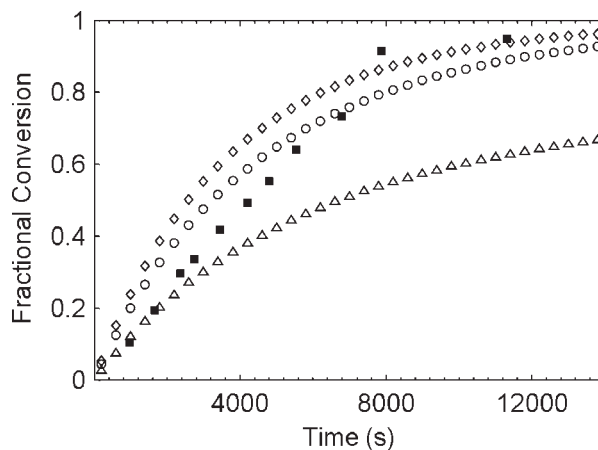
Figure 9. Conversion versus time from KMC simulation using styrene at 75 °C and a particle diameter of 170 nm, with $k_{t,m} = 54.3$ s^{-1}, $f = 0.6$, and desorption rates of 0.0 ($\triangle$); 0.05 $k_{p,m}N_{m,0}$ ($\diamondsuit$); 3.0 $k_{p,m}N_{m,0}$ ($\bigcirc$), with Alduncin and Asua's conversion versus time data[13] ($\blacksquare$).

Using the previously described method for calculating styrene diffusivity, a monomer diffusivity of 2.81×10^{-5} cm^2/s is obtained at 50 °C. The increase in probability of propagation prior to desorption when increasing the temperature from 50 to 75 °C is calculated as $(k_{p,m,75\,°C}N_{m,0}/D_{75\,°C})/(k_{p,m,50\,°C}N_{m,0}/D_{50\,°C})$, which is $(4641/3.77 \times 10^{-5})/(1999/2.81 \times 10^{-5}) = 1.73$. Thus, a radical is nearly twice as likely to propagate before desorption when the temperature is increased from 50 to 75 °C. The increase in particle diameter, using a 170-nm particle to compare with Asua's data and a 109-nm particle for our data, is by a factor of 1.6, and so the combined effect of the propagation rate and particle size shows that a radical should be 3.5 times less likely to desorb from a particle using Asua's experimental data compared with our own. Other effects we did not consider, such as interactions of radicals with the surfactant or costabilizer on the particle surface, may increase with temperature and further reduce the rate of radical desorption, or result in fast readsorption.

CONCLUSIONS

Both the experimental and simulation results presented here support the hypothesis that absorption of aqueous-phase radicals is insignificant in the miniemulsion polymerization of styrene, whether such radicals desorb from particles or are generated in the aqueous phase. This conclusion does not wholly contradict the work of Nomura and Suzuki,[6] because he examined nucleation in both micro- and macroemulsion polymerization, where nucleation primarily occurs in the smaller micelles. The results of the KMC simulations compared with our data show that chain transfer, mechanism (iii), is dominant at our experimental conditions and particle diameter. The results of the KMC simulations compared with the data of Alduncin and Asua,[13] along with the molecular weights predicted for mechanisms (i) and (ii), show that simple termination, mechanism (i), is dominant at their experimental conditions, with mechanism (ii) also playing a role. Desorption of radicals is affected by both temperature and particle size, increasing with both decreased temperature and decreased particle size. This conclusion substantiates the central idea of Asua's theory of particle nucleation, under certain experimental conditions, although chain transfer to monomer is shown here to be unnecessary for radical desorption. Based on this model-

ing work, it appears that no single mechanism is always dominant in miniemulsions, but that the interplay between mechanisms is significant, and that the significance of each depends on the details of the recipe. The KMC simulation of miniemulsion particles is shown to be an effective method for examining the mechanisms involved in particle nucleation using oil-soluble initiators. Unlike most previously used modeling approaches for miniemulsions, it considers stochastic effects due to the small numbers of species in a particle, and it enables the prediction of conversion and molecular weight distribution.

NOMENCLATURE

D	Diffusivity, cm^2/s
E_i	Number of possible events of type i in KMC algorithm
f	Initiator efficiency
$[I]$	Initiator concentration in particle, mol/L
j_{crit}	Critical chain length for radical entry
$k_{abs,m}$	Molecular absorption rate constant, s^{-1}
k_d	Initiator dissociation rate constant, s^{-1}
$k_{des,m}$	Molecular desorption rate constant, s^{-1}
K_i	Rate for event of type i in KMC algorithm
k_p	Propagation rate constant, L/mol/s
$k_{p,m}$	Molecular propagation rate constant, s^{-1}
K_{sum}	Sum of rates for all possible events in KMC algorithm
k_t	Termination rate constant, L/mol/s
$k_{t,m}$	Molecular termination rate constant, s^{-1}
k_{tr}	Chain transfer rate constant, L/mol/s
$k_{tr,m}$	Molecular chain transfer rate constant, s^{-1}
$[M]$	Monomer concentration in particle, mol/L
MW_{sty}	Molecular weight of styrene, 104.15 g/mol
n	Number of radicals per particle
$\overline{n}$	Average number of radicals per particle
n_{aq}	Number of aqueous-phase radicals per particle
n_I	Concentration of initiator in water, mol/L
N_I	Number of initiator molecules per particle
N_m	Number of monomers in particle
$N_{m,0}$	Initial number of monomers in particle
N_{pairs}	Number of radical pairs per particle
N_T	Number of particles per L of water
N_A	Avogadro's number
r_{abs}	Radical absorption rate
r_d	Initiator dissociation rate, mol/L/s
r_{des}	Radical desorption rate
r_p	Propagation rate, mol/L/s
r_t	Termination rate, mol/L/s

r_{tr}	Chain transfer rate, mol/L/s
$[R*]$	Radical concentration in particle, mol/L
T	Temperature
V_p	Particle volume, L
x_r	Uniformly distributed random number on the interval (0,1)
τ	Time step for each event in KMC algorithm

REFERENCES AND NOTES

1. Schork, F. J.; Luo, Y. W.; Smulders, W.; Russum, J. P.; Butte, A.; Fontenot, K. In Polymer Particles, Advances in Polymer Science; Okubo, M., Ed.; Springer-Verlag: Berlin, 2005; Vol. 175, Chapter: Miniemulsion Polymerization, pp 129–256.

2. Asua, J. M. Prog Polym Sci 2002, 27, 1283–1346.

3. Chern, C. S.; Poehlein, G. W. J Polym Sci Part A: Polym Chem 1987, 25, 617–635.

4. Krywko, W. P.; McAuley, K. B.; Cunningham, M. F. Polym React Eng 2002, 10, 135–161.

5. Asua, J. M.; Rodriguez, V. S.; Sudol, E. D.; El-Aasser, M. S. J Polym Sci Part A: Polym Chem 1989, 27, 3569–3587.

6. Nomura, M.; Suzuki, K. Ind Eng Chem Res 2005, 44, 2561–2567.

7. Karlsson, O. J.; Stubbs, J. M.; Carrier, R. H.; Sundberg, D. C. Polym React Eng 2003, 11, 589–625.

8. Prescott, S. W. Macromolecules 2003, 36, 9608–9621.

9. Luo, Y. W.; Yu, B. Polym Plast Technol Eng 2004, 43, 1299–1321.

10. Piton, M. C.; Gilbert, R. G.; Chapman, B. E.; Kuchel, P. W. Macromolecules 1993, 26, 4472–4477.

11. Arcos-Casarrubias, J. A.; Olayo, R. J Polym Sci Part B: Polym Phys 2003, 41, 1605–1614.

12. Pickup, S.; Blum, F. D. Macromolecules 1989, 22, 3961–3968.

13. Alduncin, J. A.; Asua, J. M. Polymer 1994, 35, 3758–3765.

14. Buback, M.; Gilbert, R. G.; Hutchinson, R. A.; Klumperman, B.; Kuchta, F. D.; Manders, B. G.; O'Driscoll, K. F.; Russell, G. T.; Schweer, J. Macromol Chem Phys 1995, 196, 3267–3280.

15. Zetterlund, P. B.; Saka, Y.; McHale, R.; Nakamura, T.; Aldabbagh, F.; Okubo, M. Polymer 2006, 47, 7900–7908.

16. Breitenbach, J. W.; Schindler, A. Monatsh Chem 1952, 83, 724–730.

17. Patnode, W.; Scheiber, W. J. J Am Chem Soc 1939, 61, 3449–3451.

18. Matheson, M. S.; Auer, E. E.; Bevilacqua, E. B.; Hart, E. J. J Am Chem Soc 1951, 73, 1700–1706.

19. Lane, W. H. Ind Eng Chem: Anal Ed 1946, 18, 295–296.

20. Dong, Y.; Sundberg, D. C. Macromolecules 2002, 35, 8185–8190.

21. Nomura, M.; Ikoma, J.; Fujita, K. J Polym Sci Part A: Polym Chem 1993, 31, 2103–2113.

22. Fichthorn, K. A.; Weinberg, W. H. J Chem Phys 1991, 95, 1090–1096.

23. Chatterjee, A.; Vlachos, D. G. J Comput Aided Mater Des 2007, 14, 253–308.